FACTA UNIVERSITATIS
Series: **Mechanical Engineering** Vol. 21, Nº 1, 2023, pp. 101 - 120
https://doi.org/10.22190/FUME210412055K

Original scientific paper

SPRING BASED ON FLAT PERMANENT MAGNETS: DESIGN, ANALYSIS AND USE IN VARIABLE STIFFNESS ACTUATOR

Bartłomiej Kozakiewicz, Tomasz Winiarski

Warsaw University of Technology, Institute of Control and Computation Engineering, Poland

Abstract. *Modern robot applications benefit from including variable stiffness actuators (VSA) in the kinematic chain. In this paper, we focus on VSA utilizing a magnetic spring made of two coaxial rings divided into alternately magnetized sections. The torque generated between the rings is opposite to the angular deflection from equilibrium and its value increases as the deflection grows – within a specific range of angles that we call a stable range. Beyond the stable range, the spring exhibits negative stiffness what causes problems with prediction and control. In order to avoid it, it is convenient to operate within a narrower range of angles that we call a safe range. The magnetic springs proposed so far utilize few pairs of arc magnets, and their safe ranges are significantly smaller than the stable ones. In order to broaden the safe range, we propose a different design of the magnetic spring, which is composed of flat magnets, as well as a new arrangement of VSA (called ATTRACTOR) utilizing the proposed spring. Correctness and usability of the concept are verified in FEM analyses and experiments performed on constructed VSA, which led to formulating models of the magnetic spring. The results show that choosing flat magnets over arc ones enables shaping spring characteristics in a way that broadens the safe range. An additional benefit is lowered cost, and the main disadvantage is a reduced maximal torque that the spring is capable of transmitting. The whole VSA can be perceived as promising construction for further development, miniaturization and possible application in modern robotic mechanisms.*

Key Words: *Variable Stiffness Actuator, Elastic Joint, Magnetic Spring, Magnetic Clutch, Soft Robotics*

1. INTRODUCTION

Construction of most of kinematic chains of robots, which are currently produced, is optimized to maximize their stiffness. Low compliance of robot links and joints is especially vital in typical industrial applications like welding, gluing, dispensing, picking and placing

Received April 12, 2021 / Accepted July 16, 2021
Corresponding author: Tomasz Winiarski
Warsaw University of Technology, Institute of Control and Computation Engineering, Nowowiejska 15/19, 00-665 Warsaw, Poland
E-mail: tomasz.winiarski@pw.edu.pl

because it plays a crucial role in providing high accuracy of the end effector positioning and avoiding undesired oscillations [1]. However, there is a significant downside to this approach – increasing rigidity of kinematic chain results in reducing its potential for safe energy absorption. Consequently, due to safety standards, such robots should either have their performance limited or work in safety zones to minimize the risk of collisions. In a context of growing interest in utilizing robots that would be capable of direct cooperation with humans (also in industrial applications) [2], it seems reasonable to intentionally include compliance in the kinematic chain as a means which potentially reduces negative consequences of collision [3–6]. As stated before, the price for that is positioning accuracy. A practical compromise is to make compliance controllable by using variable stiffness actuators (VSA) and to implement a soft-arm tactics [7], which is to perform fast rough movements in safe compliant state and slow precise ones in the more accurate stiff configuration.

Including compliance in a mechanism – especially when it is variable and controllable – may have some other beneficial consequences [8]. First of all, the capability of energy absorption makes a new class of advanced movements possible, e.g. effective throwing and catching, walking and jumping [9]. Some of them like ball kicking and running require adjusting stiffness between consecutive phases of movement [10–12]. Moreover, achievable forces [4] and velocities [3, 13] are greater in the case of compliant mechanisms than in the stiff ones. Last but not least, the resonance frequency of the elastic kinematic chain can be adjusted to its working cycle resulting in reduced energy consumption [14–16]. All these factors explain why human body actuators, which are antagonistic pairs of muscles, are also capable of in-fly stiffness adjustment [17].

Most VSA designs can be assigned to one of three categories [18]:

A. stiff constructions controlled in a way that enforces compliant behavior,
B. compliant construction controlled in a way that enforces stiffness variability,
C. compliant constructions which stiffness is adjusted mechanically.

Actuators from the first group are the most popular, especially in a field of service and assisting robots – where the safety issues are particularly important [19–21]. This is one of the reasons for the active development of suitable arm control algorithms, which include mechanical interactions with the environment – especially humans. Some significant achievements are based on either impedance control [22–24] or force control [25–29]. It is worth noting that there are also some commercially available robots for professional industrial use equipped with VSAs belonging to this category [30].

There are not so many constructions belonging to the second group (B) because they are mechanically more complicated than those from the first group, and provide not so many benefits as those from the third group. Some notable examples are [31, 32].

It is only possible for the constructions belonging to category C to fully utilize compliant parts capability of energy storage, what makes this specific group peculiarly attractive in the context of the previously mentioned benefits. There are three main methods of achieving stiffness variability by mechanical means [18, 33]:

C1. changing pretension of non-linear compliant components (often arranged in an antagonistic way [34]) – e.g. varying air pressure in a pair of pneumatic muscles,
C2. changing transmission between the compliant component and output link – e.g. moving pivot point of a lever connecting spring with output arm,
C3. changing parameters of compliant component – e.g. adjusting the active length of a leaf spring or its second moment of area.

In all these categories, the most frequently used compliant components are leaf springs, helix springs and elastic rods [18]. An interesting alternative is to use magnetic parts. The concept of replacing mechanical components with their magnetic equivalents is already present in different branches of engineering. Some notable examples are magnetic bearings [35], magnetic clutches and magnetic transmissions [36]. A summary of previous achievements in constructing magnetic springs is presented in Section 2.

In this paper, we propose a design of magnetic torsional spring composed of flat magnets and also a conception of its application in variable stiffness actuator. The proposed solution increases the scope of magnetic springs applicability in a context of VSAs development by increasing ranges of angles for which spring torque-angle characteristics are stable and close to linear. The idea is supported by an analysis of magnetic spring dynamic behavior and its dependency on torque-angle characteristics (Section 3). The effect of the proposed solution (Section 4) is verified in FEM analysis (Section 5) and multiple experiments conducted on constructed VSA (Section 6). Their results were used to develop mathematical models of magnetic spring discussed in Section 7. Section 8 summarizes the work.

2. Related Work

Numerous conceptions of compliant mechanisms based on magnetic components have been developed so far. Some of them refer to non-linear springs consisting of magnets in various arrangements which potentially can be used in antagonistic VSAs classified in C1 group [37, 38]. At least one conception was successfully implemented in such a setup [39]. A different approach is to use electromagnets and adjust system stiffness by changing current applied to them [40, 41]. Such construction belongs to C3 group, but it has one major drawback – high energy consumption also in steady state.

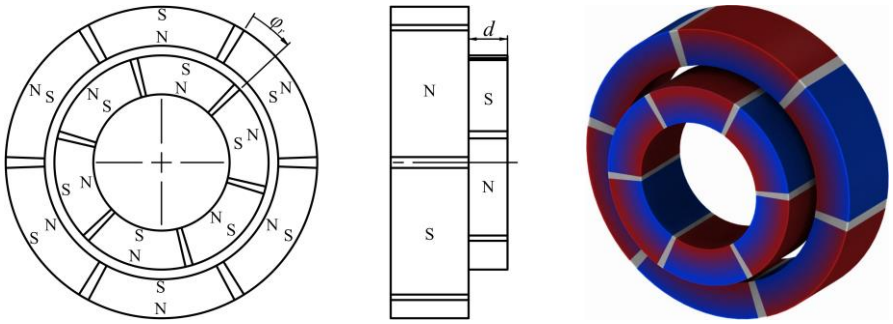

Fig. 1 Variable stiffness torsional spring based on arc magnets – AMS

Another interesting solution belonging to C3 category is shown in Fig. 1. It presents a variable stiffness torsional spring, which is made of two coaxial rings consisting of radially magnetized arc magnets aligned in an alternating way. When the components are in equilibrium, rotating one of the rings results in counter-acting torque τ_{sp} whose value is approximately proportional to angle φ_r between the rings if the angle is sufficiently small. Stiffness adjustment can be accomplished by translating one of the rings along the axis. Moving rings away from the equilibrium by a distance d causes the overlapping part to

become smaller, which reduces magnetic forces between the rings and hence the stiffness of the system decreases. We will refer to this solution as AMS – Arc Magnets Spring.

Such an arrangement has some unique advantages like decoupled position and stiffness control, no need for constant energy supply, inherent maximum torque limit, possible zero stiffness configuration (rings completely decoupled) and an unlimited angular position range. It also has some benefits which are typical for solutions based on magnets: no contact between moving parts, reduced friction and wear, and zero clearances between cooperating parts.

To the best of our knowledge, the AMS arrangement has been proposed for the first time in [42]. Authors of that paper built a magnetic spring using four arc magnets per ring, implemented it in construction of VSA and measured some characteristics like torque-angle relationship for different axial distances between the rings. A continuation of that work was a development of a modified design of a more compact spring [43] with an additional intermediary ring used to increase its maximal torque.

The other significant achievement in this field has been made by authors of the paper [44]. They prepared and performed multiple FEM analyses for different arrangements of magnets in AMS – in particular, they examined an impact of poles number and magnets dimensions on maximum torque, energy and stiffness of magnetic spring. To verify the simulation model, the authors built simple two poles spring and measured its characteristics.

3. Magnetic Spring Characteristics

Despite of all of the advantages of the arc magnetic springs they have at least one major drawback – they exhibit unstable behavior for specific angles φ_r. To examine that phenomenon in detail, we shall introduce some additional terms. Fig. 2 presents sample torque-angle characteristics of magnetic spring. When external load τ_{ld} (whose value is lower than maximal torque) is applied to one of the rings, multiple equilibrium points occur. If term $d\tau_{sp}/d\varphi_r$ has a negative sign, the whole system acts like a conventional torsional spring and equilibrium is stable. Otherwise, even a small change of resultant torque causes the system to move away from equilibrium, which in this case is unstable, and to accelerate toward the next stable one. The direction of this movement depends heavily on initial disturbance, which makes it nearly impossible to predict and – as a consequence – problematic to control. For this reason, it is better to avoid unstable regions of spring characteristic in typical applications. The critical angle, separating stable and unstable regions, corresponds to maximal torque. To make sure that it is not exceeded, it may be necessary to assume some safety margin and to operate only within the safe range of angles which is narrower than the stable one.

It may be beneficial to utilize even a tinier span of angles. Control laws could be much simpler if the relationship between torque and deflection were linear (stiffness irrelevant to angle). In fact, in multiple papers concerning modeling and control of robots with compliant joints, the linearity of compliance is one of the main assumptions [45–47]. The range of angles which provides that real characteristic differs from the linearised one no more than 5% we will call a linearity range.

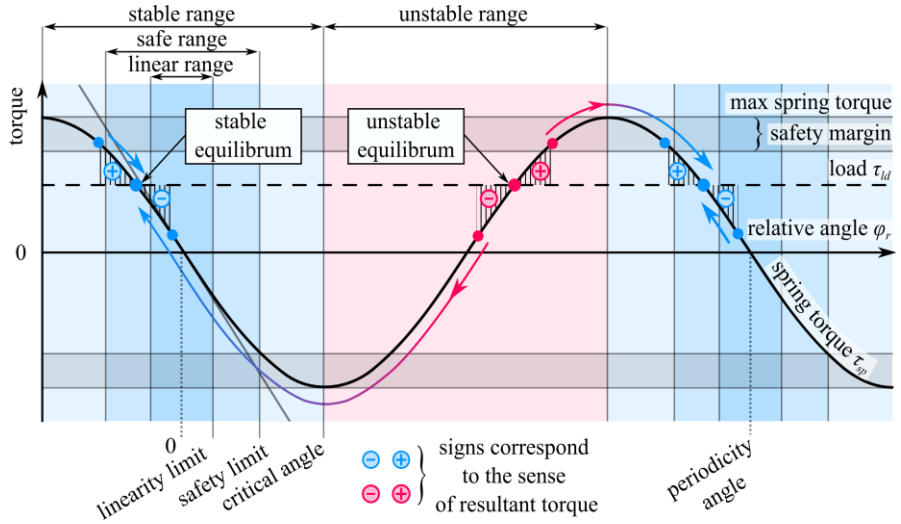

Fig. 2 Terms describing torque-angle characteristics of magnetic spring

The part of the stable range of angles that can be utilized as a safe or linear range depends on the shape of torque-angle characteristics (Fig. 3). A typical plot for a many-pole magnetic spring is close to sinusoid (curve 2). The fewer the poles, the more trapezoidal (curve 1) or even rectangular alike the shape becomes [44] making safe and linear ranges exceptionally narrow. In this context, a triangular (curve 3) or saw (curve 4) alike form of a curve would be more beneficial, however – to the best of our knowledge – it has not been obtained for arc magnets springs so far. In this paper, we propose a solution to broaden both linear and safe ranges of magnetic spring.

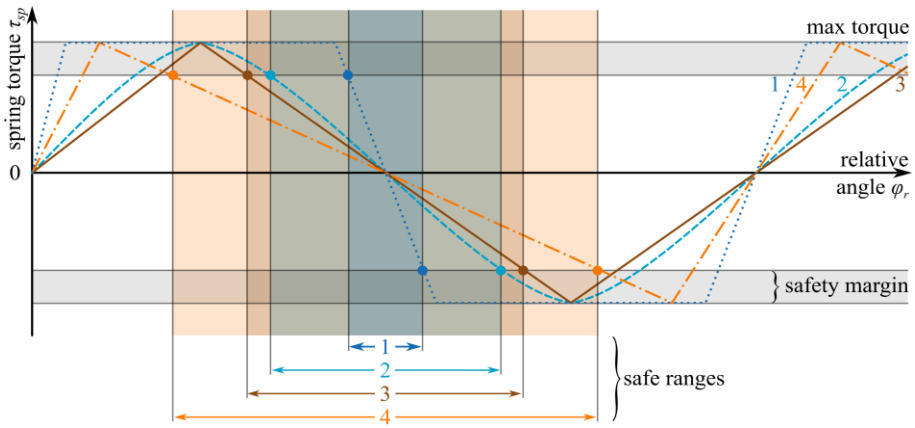

Fig. 3 Impact of torque-angle characteristics shape on widths of safe ranges of angles

4. CONCEPTION OF VSA BASED ON FLAT PERMANENT MAGNETS

The trapezoidal shape of few-poles-AMS torque-angle characteristics is related to a non-linear way the magnetic field distribution changes as the rings rotate relative to each other. The idea that we propose is to alter air gap width with respect to the relative angle in a way that compensates these non-linearities and results in a more triangular form of characteristics. A specific configuration of magnets that we suggest is presented in Fig. 4.

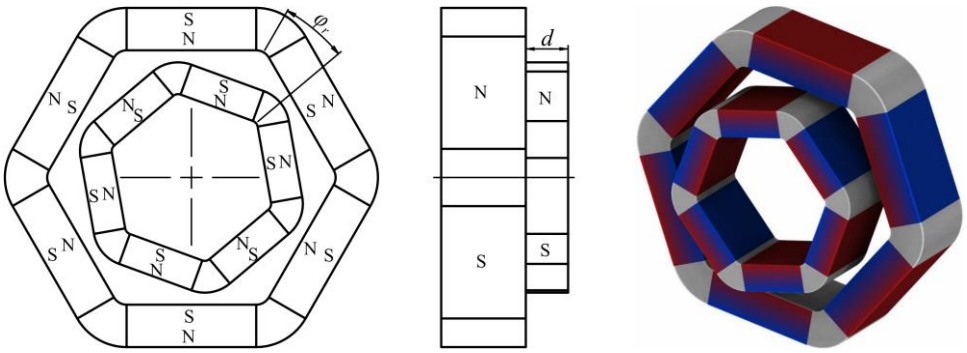

Fig. 4 Proposed variable stiffness torsional spring based on flat magnets – FMS

The rings are composed of flat magnets aligned into polygons and magnetized in a direction perpendicular to their walls. We will call this setup FMS – Flat Magnets Spring. As will be proven in this paper, it is possible to obtain the effect described above by proper choice of polygon and magnets dimensions.

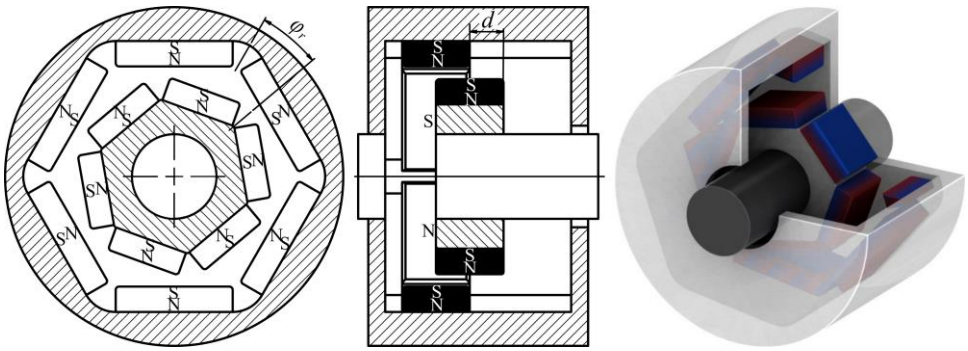

Fig. 5 Practical setup of magnetic rings

While Fig. 4 depicts the general conception of magnets arrangement, Fig. 5 presents more practical setup visualizing one of the possible ways of supporting cooperating components on shafts and of enclosing the whole assembly to separate it physically and magnetically from its environment. Magnets in the outer ring are attached to a ferromagnetic tube with ferromagnetic cups on both ends, while magnets in the inner ring are attached to a ferromagnetic drilled core. Both components are mounted to non-ferromagnetic shafts. Such a choice of materials results in high magnetic flux density in the

inside of the spring and a negligibly small stream leakage to the outside as it was proved in simulation described in Section 5. Fig. 6 presents a proposed conceptual design of variable stiffness actuator based on magnetic spring. We will refer to this setup as ATTRACTOR – vAriable sTiffness magneTic spRing ACTuatOR.

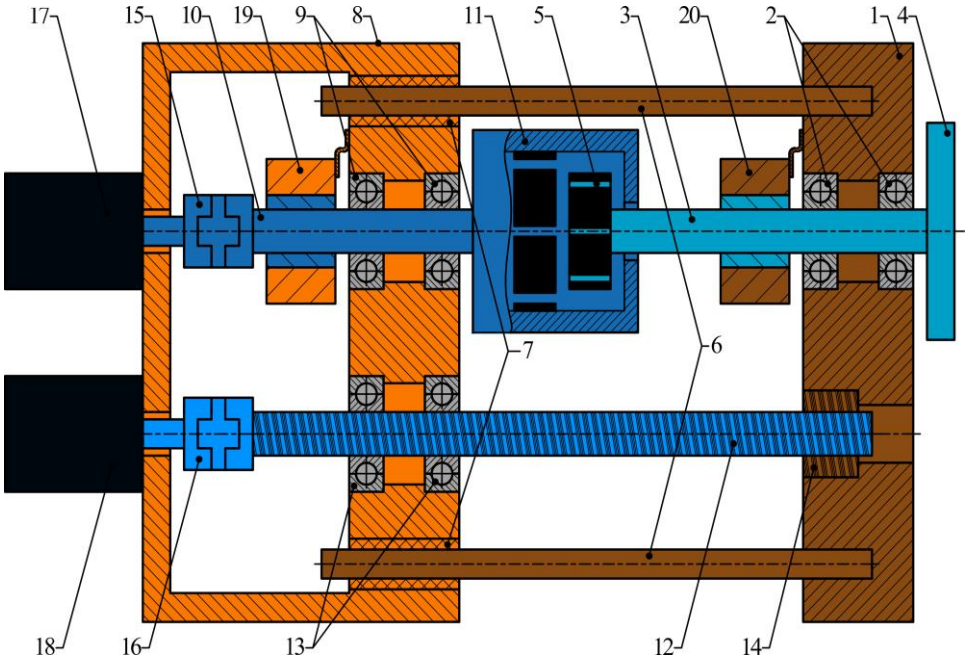

Fig. 6 VSA concept – ATTRACTOR: 1. fixed frame, 2. bearings, 3. output shaft, 4. flange, 5. inner magnetic ring, 6. guiding shafts, 7. linear bushings, 8. rigid carriage, 9. bearings, 10. input shaft, 11. outer magnetic ring, 12. lead screw, 13. bearings, 14. nut, 15,16. clutches, 17,18. DC servomotors, 19,20. absolute optic encoders

5. SIMULATION

There were three main goals of FEM analyses performed on magnetic spring models: verifying a choice of materials presented in Section 4, investigating an impact of magnets number, shape and arrangement on spring torque-angle characteristics and optimizing dimensions of spring used in experiments.

Multiple models of AMS and FMS were prepared to perform FEM analyses. Investigated cases differed from each other with number of poles. All the AMS models had the same overall dimensions. In the case of FMS, it was impossible to obtain that, so only the inner dimensions (in Fig. 7 marked as g, l, w and z) were kept the same. The geometry and dimensions of analyzed models are presented in Fig. 7 and specific values are summarized in Table 1. Material properties were assigned to components according to the description in Section 4 and the values presented in Table 2. In each case, the spring was surrounded by an air cylinder with Neumann boundary conditions on its surface.

Table 1 Specific values of dimensions of investigated spring models [mm] (parameters which varied across simulations are bold)

Spring type	**Pole pairs**	g	l	**u**	w	z	G	H_1	H_2	L	P_1	P_2	**U**	**W**	**Z**	**s**	t
AMS	**2**	4	40	**88°**	32	44	4	8	3	84	20	20	**88°**	**63**	**75**	**4.0**	2
	3	4	40	**58°**	32	44	4	8	3	84	20	20	**58°**	**63**	**75**	**4.0**	2
	4	4	40	**43°**	32	44	4	8	3	84	20	20	**43°**	**63**	**75**	**4.0**	2
FMS	**2**	4	40	**30**	32	44	4	8	3	84	20	20	**40**	**71**	**84**	**5.5**	2
	3	4	40	**20**	32	44	4	8	3	84	20	20	**30**	**67**	**74**	**3.4**	2
	4	4	40	**16**	32	44	4	8	3	84	20	20	**20**	**65**	**70**	**2.7**	2

Table 2 Material properties

Material	Air	Aluminum	Struct. steel	NdFe35
Isotropic relative permeability μ_r [-]	1.00	1.00	10000	1.10
Magnetic coercivity H_m [kAm^{-1}]	0	0	0	890

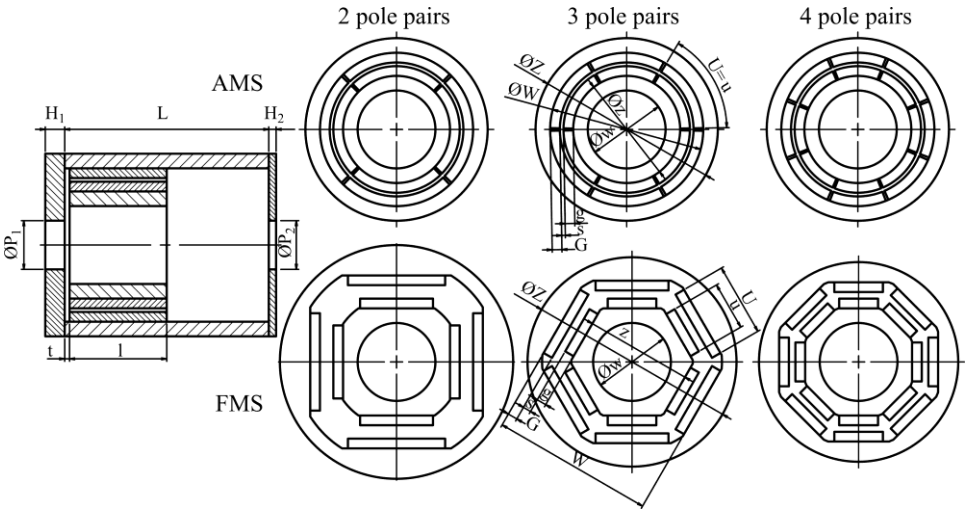

Fig. 7 Shapes and dimensions of investigated spring models (up to scale)

An initial analysis was performed to investigate the impact of rings material on magnetic flux density. The results are presented in Fig. 8, and they confirm the theses stated in Section 4. Hence, the material of supporting rings was set as structural steel.

In the following analyses, the investigated quantities were torque and axial force between the rings calculated using the virtual work principle [48] for different values of relative angle and distance. Fig. 9a presents resultant torque-angle characteristics obtained in a configuration of maximal stiffness (d = 0). Examined FMSs have lower maximal torque and stiffness than AMSs of the same number of poles and similar dimensions. The fewer the poles, the difference becomes more significant. Fig. 9b visualizes the data normalized – torque is described as a fraction of maximal torque and angle as a fraction of stability limit angle. Such representation enables a comparison of characteristics shapes.

As expected, investigated FMSs provide characteristics of more triangular form than AMSs. Again, the fewer the poles, the difference becomes more significant.

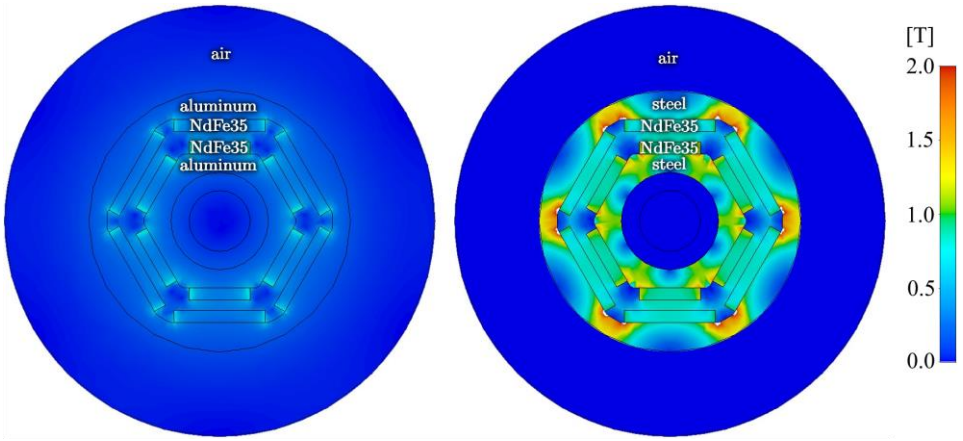

Fig. 8 Impact of rings material on magnetic flux density

The case arbitrarily selected for further investigation was 6-pole FMS. Multiple analyses were performed to limit maximal torque of the selected spring below stall torque of the available drive and to maximize the linear and the safe range of angles. The optimization variables were all dimensions listed in Table 1. The constraints were a result of space limits and availability of prefabricated components. The resultant characteristics are presented in Fig. 9 (labeled as "final").

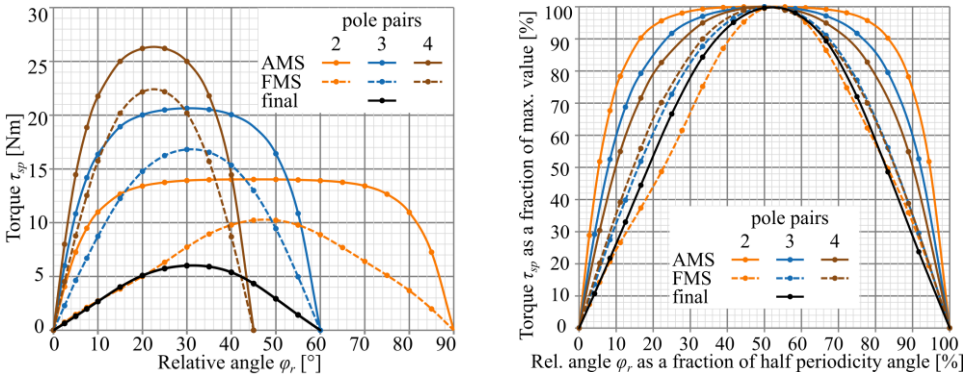

a) Not normalized **b)** Normalized

Fig. 9 FEM analyses results: torque-angle characteristics for $d = 0$

6. EXPERIMENTS

The conceptions presented in Section 4 and dimensions optimized in Section 5 were used to design and build magnetic spring (Fig. 10a), as well as variable stiffness actuator following ATTRACTOR concept (Fig. 10b and Fig. 10c).

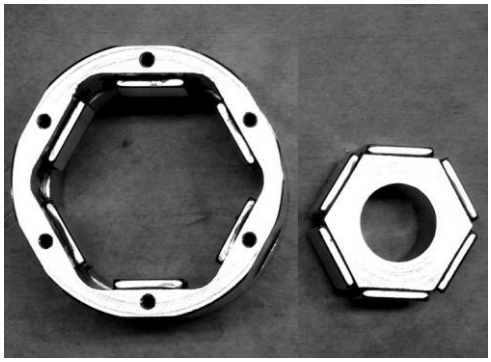

a) Outer and inner magnetic ring

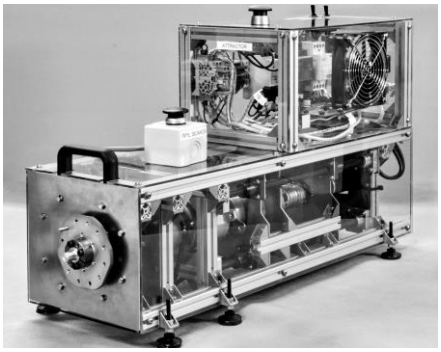

b) ATTRACTOR

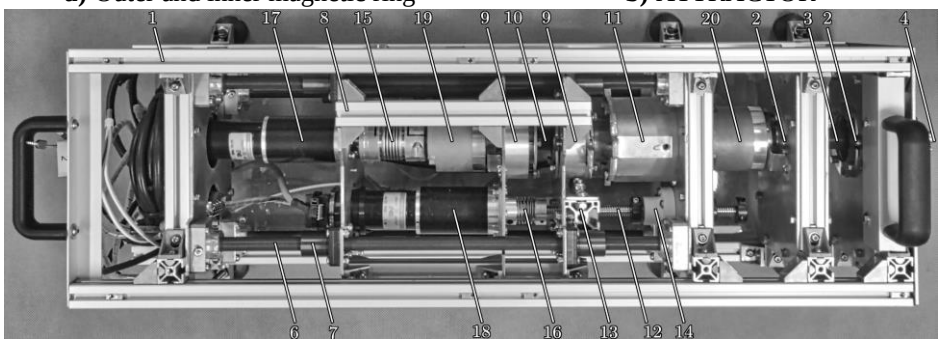

c) ATTRACTOR components (numbers correspond to Fig. 6)

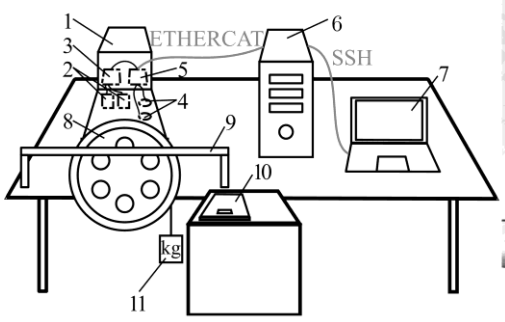

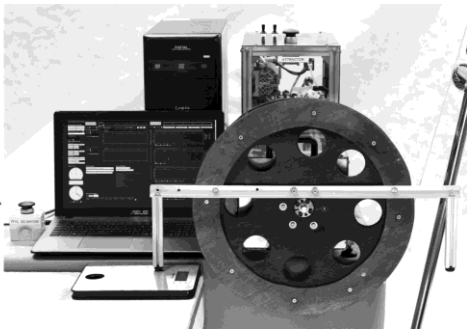

d) Experimental setup: 1. ATTRACTOR, 2. DC servomotors, 3. driver, 4. encoders, 5. controller gathering data from encoders, 6. PC with RTOS supervising the experiments, 7. PC used to design experiments and analyze their results, 8. flywheel, 9. removable lever arm, 10. scale, 11. mass hung on a cord wound on the flywheel

Fig. 10 Constructed device

Some additional equipment mountable to the output flange was prepared: flywheel used to increase inertia in order to slow down device dynamics and lever arm used to interact with the output shaft. The whole experimental setup is presented in Fig. 10d. The methodology of conducted experiments is described in Section 6.1, while their results and analysis are presented in Section 6.2.

6.1. Methodology

The experiments conducted on ATTRACTOR mechanism can be divided into three categories: one examining the torque-angle relationship of the spring (experiment A), one focused on identifying basic mechanical properties of the system (experiment B) and the last oriented on developing a model of the whole joint – understood as a relationship between position trajectories of output shaft $\varphi_{out}(t)$ and input shaft $\varphi_{in}(t)$ (experiment C).

A methodology of **experiment A** was to apply torque to input shaft using DC motor, to estimate its value τ_{sp} basing on indications of rigidly fixed scale pushed with lever arm and to estimate relative angle φ_r by subtracting readings of absolute encoders mounted on shafts φ_{out}-φ_{in}. The whole procedure was repeated for different axial distances d between the magnetic rings and all three stable equilibria. Due to the instability described in Section 3, the range of examined angles was limited (-41° ÷ 41° from stable equilibrium), but it was broader than the stable range (-31.5° ÷ 31.5°) because of static friction.

Experiment B was performed to identify aggregate inertia J of the output shaft and all components rigidly mounted to it. Different masses m were hung on a cord wound on the flywheel and dropped. Angular acceleration of output shaft ($\ddot{\varphi}_{out}$) was estimated by analyzing encoders readings. The experiment was performed with completely decoupled shafts, so only the parts connected to the output shaft were rotating.

Experiment C consisted of multiple trials. Their goal was to excite system in different ways by providing current profiles $i(t)$ of various shapes (sinusoid, square, step, impulse function) to the motor and to gather information about movements of both shafts $\varphi_{out}(t)$, $\varphi_{in}(t)$ for different distances d. The data were split into two equinumerous sets: teaching and verifying and were used to develop and fit the model of the joint.

6.2. Results and analysis

Data gathered in experiment A was used to find a model of the relationship between spring torque τ_{sp} and relative distance d and angle φ_r between the rings. Various general approximating functions were considered: polynomials of different order and number of variables and Fourier series terms. The best results were obtained for the model described with Eq. (1) and discussed in Section 7.1:

$$\tau_{sp}(d,\varphi_r) = -\left(1 + a_1 d + a_2 d^2 + a_3 d^3 + a_4 d^4\right)\left(b_1 \sin\left(\frac{\pi}{60}\varphi_r\right) + b_2 \sin\left(\frac{\pi}{30}\varphi_r\right) + b_3 \sin\left(\frac{\pi}{15}\varphi_r\right)\right) \quad (1)$$

where τ_{sp} denotes estimated spring torque, d and φ_r refer to the distance and the angle between the rings, and $a_{...}$, $b_{...}$ are model parameters. An excerpt of gathered data (marked as dots) and fitted surface described by Eq. (1) are presented in Fig. 11. Spring stiffness for small angles φ_r can be described with Eq. (2) obtained as a partial derivative of Eq. (1).

$$k_{sp}(d) = -\frac{\partial \tau_{sp}(d,\varphi_r)}{\partial \varphi_r}\bigg|_{\varphi_r=0} = \left(b_1\frac{\pi}{60} + b_2\frac{\pi}{30} + b_3\frac{\pi}{15}\right)\left(1 + a_1 d + a_2 d^2 + a_3 d^3 + a_4 d^4\right) \quad (2)$$

Eq. (3), which is derived from the Euler equation of rotary motion, represents a simple model of a relationship between output shaft acceleration $\ddot{\varphi}_{out}$ on dropped mass m.

$$\ddot{\varphi}_{out} = \frac{mgr - \tau_{fr}}{mr^2 + J} \quad (3)$$

$\ddot{\varphi}_{out}$ denotes an angular acceleration of output shaft, m – mass attached to the flywheel, g – gravitational acceleration, r – flywheel radius, τ_{fr} – friction torque, J – inertia.

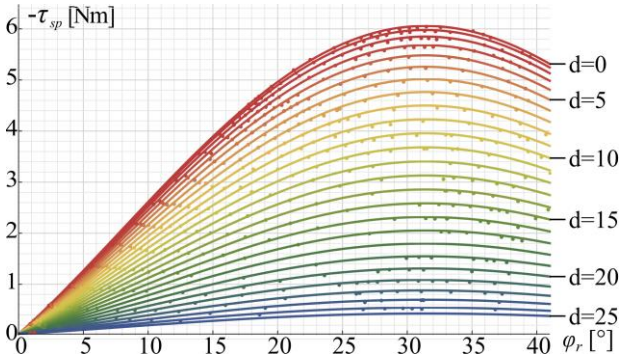

Fig. 11 Torque-angle relationship for different distances between the rings

Inertia J of output shaft was identified by fitting function (3) to the data gathered in experiment B. Radius r was known, and friction torque τ_{fr} was assumed to be independent of angular position and velocity of output shaft (Coulomb's model of solid friction), and was identified as a second parameter of the fitted model. The fitted curve is presented in Fig. 12.

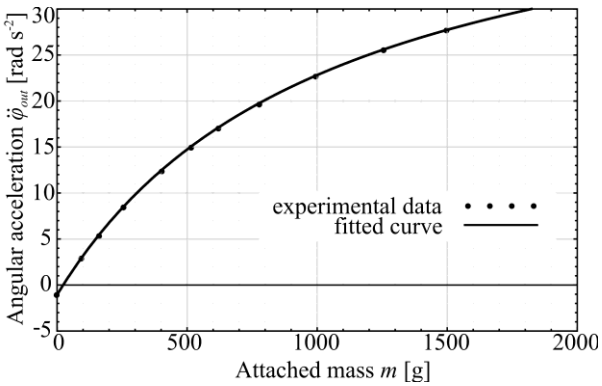

Fig. 12 The curve fitted to the results of experiment B to identify inertia and friction

If the joint were rigid, the output shaft would always have the same angular position φ_{out} as the primary shaft φ_{in}. Compliance introduces some other kind of relationship between shaft movements. Its general form can be predicted theoretically by transforming the Euler equation of rotary motion written for the output shaft (Eq. 4):

$$\ddot{\varphi}_{out}\left(d,\varphi_{in},\varphi_{out},\dot{\varphi}_{out},...\right)=\frac{\tau_{ld}+\tau_{sp}\left(d,\varphi_{out}-\varphi_{in},...\right)+\tau_{fr}\left(\dot{\varphi}_{out},...\right)}{J} \tag{4}$$

where φ_{out} denotes an angular position of the output shaft, φ_{in} – angular position of the input shaft, τ_{ld} – external torque applied to the output shaft, τ_{sp} – spring torque, d – distance between the rings, τ_{fr} – friction torque, J – inertia of output shaft and parts mounted to it.

In this model, external load τ_{ld} was treated as known – its value was zero in the experiments. The model of spring torque $\tau_{sp}(d, \varphi_{out} - \varphi_{in})$ has already been found as well as the value of inertia J. Multiple models based on Eqs. (1), (2), (4) were developed (most interesting cases are listed in Table 3 and interpreted in Section 7.2) and investigated by fitting their parameters to teaching set (described in Section 6.1) and calculating different goodness of fit measures using verifying dataset: mean square error (MSE), adjusted coefficient of determination (R^2_{adj}) standard error (SE) and Bayesian information criterion (BIC). Also, two partially linearised models were investigated: A_L and F_L. The results are listed in Table 4.

Table 3 Models of output shaft acceleration (bold symbols denote fitted parameters)

ID	Equation
A	$\ddot{\varphi}_{out}=\frac{1}{J}\left(\tau_{sp}\left(d,\varphi_{out}-\varphi_{in}\right)\right)$
B	$\ddot{\varphi}_{out}=\frac{1}{J}\left(\tau_{sp}\left(d,\varphi_{out}-\varphi_{in}\right)-\boldsymbol{\tau_{fr}}\,\mathrm{sign}\left(\dot{\varphi}_{out}\right)\right)$
C	$\ddot{\varphi}_{out}=\frac{1}{J}\left(\tau_{sp}\left(d,\varphi_{out}-\varphi_{in}\right)-\boldsymbol{\tau_{fr}}\tanh\left(\boldsymbol{v}\dot{\varphi}_{out}\right)\right)$
D	$\ddot{\varphi}_{out}=\frac{1}{J}\left(\tau_{sp}\left(d,\varphi_{out}-\varphi_{in}\right)-\boldsymbol{\tau_{fr}}\tanh\left(\boldsymbol{v}\dot{\varphi}_{out}\right)+\boldsymbol{w}\sin\left(\varphi_{out}+\boldsymbol{x}\right)\right)$
E	$\ddot{\varphi}_{out}=\frac{1}{J}\left(\tau_{sp}\left(d,\varphi_{out}-\varphi_{in}\right)-\boldsymbol{\tau_{fr}}\tanh\left(\boldsymbol{v}\dot{\varphi}_{out}\right)+\boldsymbol{w}\sin\left(\varphi_{out}+\boldsymbol{x}\right)-\boldsymbol{y}\left(\dot{\varphi}_{in}\right)\right)$
F	$\ddot{\varphi}_{out}=\frac{1}{J}\left(\tau_{sp}\left(d,\varphi_{out}-\varphi_{in}\right)-\boldsymbol{\tau_{fr}}\tanh\left(\boldsymbol{v}\dot{\varphi}_{out}\right)+\boldsymbol{w}\sin\left(\varphi_{out}+\boldsymbol{x}\right)-\boldsymbol{z}\left(\dot{\varphi}_{out}-\dot{\varphi}_{in}\right)\right)$
A_L	$\ddot{\varphi}_{out}=\frac{1}{J}\left(k_{sp}\left(d\right)\left(\mathrm{mod}\left(\varphi_{out}-\varphi_{in}+60°,120°\right)-60°\right)\right)$
F_L	$\ddot{\varphi}_{out}=\frac{1}{J}\left(k_{sp}\left(d\right)\left(\mathrm{mod}\left(\varphi_{out}-\varphi_{in}+60°,120°\right)-60°\right)-\boldsymbol{\tau_{fr}}\tanh\left(\boldsymbol{v}\dot{\varphi}_{out}\right)+\boldsymbol{w}\sin\left(\varphi_{out}+\boldsymbol{x}\right)-\boldsymbol{z}\left(\dot{\varphi}_{out}-\dot{\varphi}_{in}\right)\right)$

Table 4 Goodness of fit of shaft acceleration models

Model	Teaching set				Verifying set			
ID	MSE	1- R^2_{adj}	SE	BIC	MSE	1- R^2_{adj}	SE	BIC
A	3522	1.895‰	59.4	164593	4175	3.046‰	64.6	179356
B	2334	1.255‰	48.3	156307	3051	2.223‰	55.2	172617
C	2270	1.221‰	47.6	155762	2976	2.169‰	54.6	172092
D	1451	0.780‰	38.1	146763	2050	1.494‰	45.3	164094
E	1423	0.765‰	37.7	146382	2021	1.473‰	45.0	163795
F	1365	0.734‰	36.9	145536	2001	1.458‰	44.7	163590
A_L	4339	2.335‰	65.9	168784	148454	92.762‰	344.2	251313
F_L	2122	1.141‰	46.1	154429	153345	94.811‰	391.6	256919

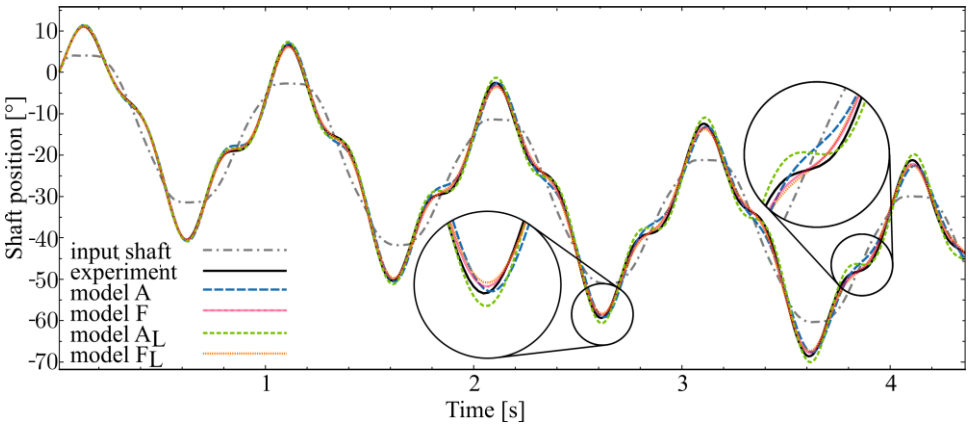

Fig. 13 Long-term output shaft trajectory simulations – not exceeding the critical angle

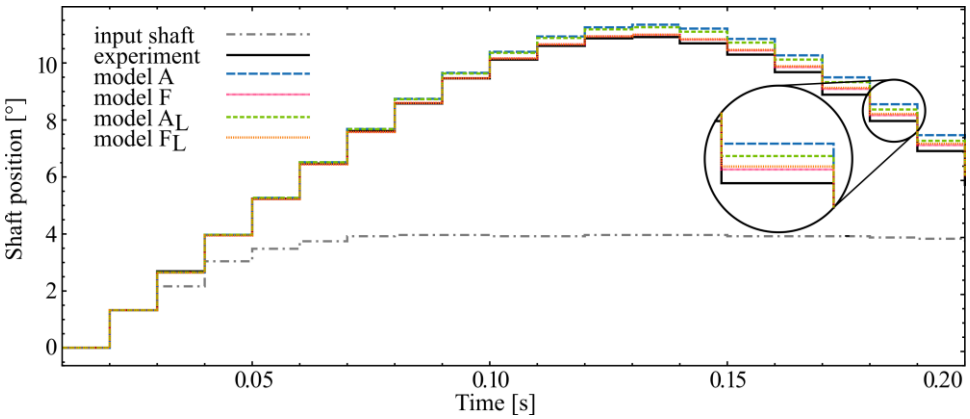

Fig. 14 Short-term output shaft trajectory simulations – not exceeding the critical angle

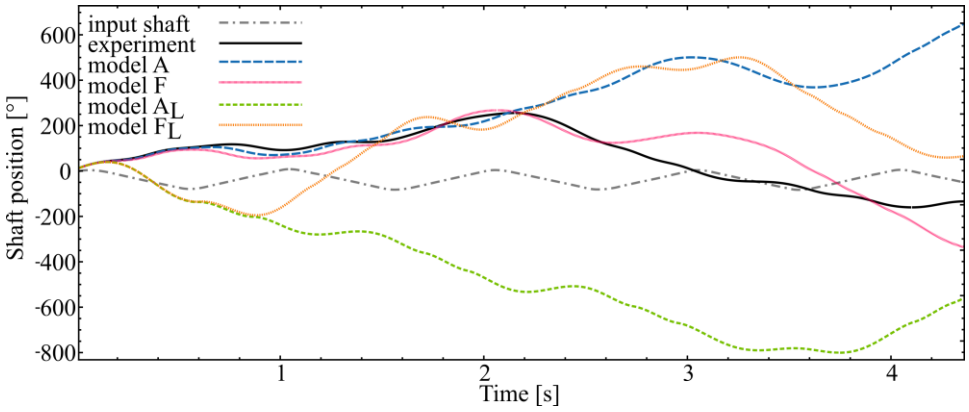

Fig. 15 Long-term output shaft trajectory simulations – exceeding the critical angle

Models listed above describe output shaft accelerations. Simple approximations (Eqs. (5) and (6)) allow deriving differential models of output shaft positions.

$$\ddot{f}(t) \approx \frac{f(t)-2f(t-T)+f(t-2T)}{T^2} \stackrel{def}{=} \frac{f^{[n]}-2f^{[n-1]}+f^{[n-2]}}{T^2} \tag{5}$$

$$\dot{f}(t) \approx \frac{f(t)-f(t-T)}{T} \stackrel{def}{=} \frac{f^{[n]}-f^{[n-1]}}{T} \tag{6}$$

For example, the position model obtained in case F is described with Eq. (7).

$$\begin{aligned}\varphi_{out}^{[n]} = 2\varphi_{out}^{[n-1]} - \varphi_{out}^{[n-2]} + \frac{T^2}{J}\Bigg(\tau_{sp}\left(d^{[n-1]}, \varphi_{out}^{[n-1]} - \varphi_{in}^{[n-1]}\right) - \tau_{fr}\tanh\left(\frac{v}{T}\left(\varphi_{out}^{[n-1]} - \varphi_{out}^{[n-2]}\right)\right) + \\ + w\sin\left(\varphi_{out}^{[n-1]} + x\right) - \frac{z}{T}\left(\varphi_{out}^{[n-1]} - \varphi_{out}^{[n-2]} - \varphi_{in}^{[n-1]} + \varphi_{in}^{[n-2]}\right)\Bigg)\end{aligned} \tag{7}$$

Position models based on acceleration models were used to simulate output shaft trajectories $\varphi_{out}(t)$ (the model was fed with its output). The simulations were performed using data from a verifying set for two classes of movements: not exceeding ($\varphi_r \leq 31.5°$) and exceeding ($\varphi_r > 31.5°$) the critical angle. The worst cases are presented in Figs. 13, 14 and 15 and discussed in Section 7.2 (to maintain readability of the figures only models A, F, A_L and F_L are included; none of the remaining models – B, C, D, E provided better performance than model F).

7. Discussion

The following sections present a discussion of the obtained results. Section 7.1 concerns spring characteristics shape and model, while Section 7.2 describes joint models interpretation and usability.

7.1. Spring characteristics

The model (Eq. (1)) of torque τ_{sp} dependency on relative angle φ_r and distance d, described in Section 6.2, has a convenient form of a product of two functions. One is a polynomial dependent on distance d, and the other is composed of the first three terms of sinus series dependant on relative angle φ_r. The model is well defined, inherently periodical, smooth and easy to analyze.

Fig. 16 presents a comparison of the surface fitted to experimental data (Eq. (1)) and results of the simulation. Curves in Fig. 16a represent torque-angle relationship for $d = 0$, while Fig. 16b depicts torque-distance relationship for $\varphi_r = 31.5°$ (points representing experimental data are plotted for $31° < \varphi_r < 32°$). The differences in the domain of angles φ_r are negligible within the stable range of angles (less than 2%); however, beyond this range, they can reach about 20%. In the domain of distances, they are much more distinct and vary from less than 5% in stiff configuration to over 40% in compliant one.

The possible reasons for the differences are modeling and numerical errors in FEM analysis, manufacturing and mounting inaccuracies, measurement errors, lack of experimental data for angles between 41° and 60° and influence of static friction. Although the last factor is unmeasurable in direct ways, its maximum value can be estimated based on the measurements gathered in experiment B – it should be close to kinetic friction identified as about 0.05Nm.

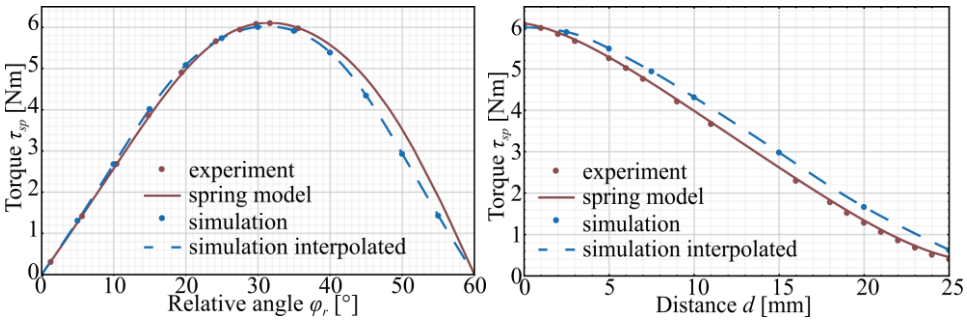

a) Torque-angle relationship **b)** Torque-distance relationship

Fig. 16 Spring characteristics – comparison of experiment and simulation

Fig. 17 presents the spring characteristics (plotted in the stiff configuration: $d = 0$) as well as its stable and linear range of angles. It is shaped as intended, and both ranges are relatively wide: their limits are 31.5° (105% of theoretical value 30°) and 19.7° (66%) accordingly. As a reference, in paper [42] where the same number of pole pairs was used these values were about: 26° (87%) and 11° (37%).

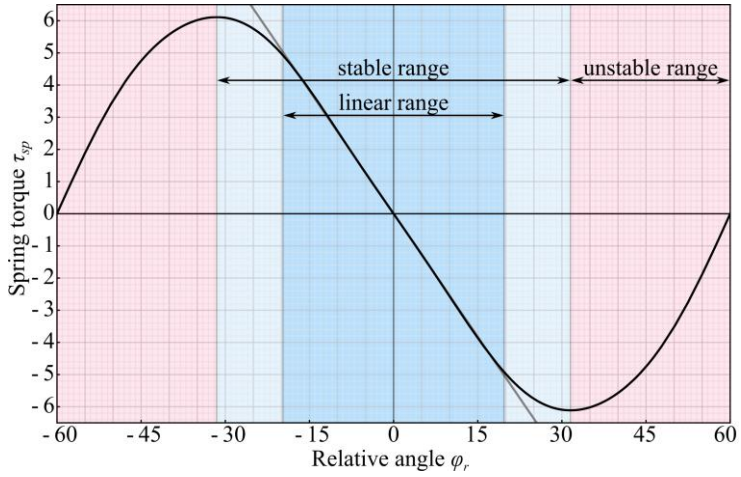

Fig. 17 Resultant torque-angle characteristics shape, linear and stable ranges

7.2. Joint model

All the models examined in Section 6.2 and listed in Table 3 have one vital feature in common – all their terms have a clear interpretation. It is summarized in Table 5.

The results presented in Table 4 indicate that the including terms corresponding to kinetic friction and wheel unbalance have a significant impact on the goodness of fit, which suggests a profound role of these factors. Implementing damping dependant on output angular velocity results in a negligible improvement, so that it can be implied that the influence of viscous friction on the output shaft movement is relatively low. Including damping dependant on relative angular velocity provides a noticeable but rather small improvement of the goodness of fit. Because there is no contact between rotating rings, the only possible explanation for such damping are magnetic interactions – probably related to inducing eddy currents in conducting components of the spring. The results indicate that – at least for investigated velocities, dimensions and mechanical parameters – this phenomenon has a relatively low impact on output shaft behavior.

The results of long-term simulations of output shaft movements (presented in Section 6.2 in Fig. 13) indicate that – provided the critical angle is not exceeded – the most complex model F can be successfully used as a long-term simulator. The same is true even for its partially linearised form F_L. If only short-term predictions are needed (Fig. 14), even the simplest models A and A_L are capable of providing satisfactory results. If the critical angle is exceeded (Fig. 15), the simulations based on non-linearised models are not satisfactorily accurate but – contrary to linearised ones – they follow the general trends of real output shaft trajectory for some period of time. This period is the longest in the case of model F (2.6 seconds in presented case). However, it is worth noting that due to the unstable behavior of magnetic spring described in Section 3, the predictability of output movement within the unstable range of angles φ_r may be inherently and inevitably limited.

Table 5 Interpretation of terms used in examined joint models

Term	Interpretation
J	inertia
$\tau_{sp}\left(d, \varphi_{out} - \varphi_{in}\right)$	static characteristics of magnetic spring
$-\tau_{fr}\operatorname{sign}\left(\dot{\varphi}_{out}\right)$	model of dry kinetic friction
$-\tau_{fr}\tanh\left(v\dot{\varphi}_{out}\right)$	differentiable approximation of the model above
$w\sin\left(\varphi_{out} + x\right)$	eccentric mass model of imperfect wheel balance
$-y\dot{\varphi}_{out}$	damping dependant on output shaft angular velocity
$-z\left(\dot{\varphi}_{out} - \dot{\varphi}_{in}\right)$	damping dependant on relative angular velocity
$k_{sp}\left(d\right)$	stiffness in stable equilibrium
$\operatorname{mod}\left(\varphi_{out} - \varphi_{in} + 60°, 120°\right) - 60°$	term providing periodicity of 120°

8. CONCLUSIONS

The experimentally verified results of simulations indicate that using flat magnets instead of arc ones for the magnetic spring construction enables alteration of its torque-angle characteristics in a beneficial way by adjusting spring geometry. In the case of a low number of magnet pairs, the choice of optimized FMS in the place of AMS results in expanding linear and stable ranges of angles, what broadens a space of movements so that the behavior of the spring is well-defined, predictable and easy to control. The additional advantage is lower cost and much better availability of flat magnets as opposed to arc ones. However, the price for all the advantages mentioned above is a reduction of spring maximal torque and stiffness. Hence, the best applications for implementing FMS are those, in the case of which the wide range of deflections and convenient control is more important than maximization of available torque. Since the more pole pairs, the lower the differences between FMS and AMS are, another field of FMS application may be constructions with high pole pairs number.

The device constructed accordingly to ATTRACTOR concept is proven in use and constitutes an example of usability of FMS arrangement in VSA development. The movement of the output shaft within the stable range of angles can be well predicted by a simple linearized model and even simulated for a more extended period using a model, which is more complex but still easy to interpret.

There is a large potential of device miniaturization what – combined with many important advantages of magnetic mechanisms like reduced wear, zero backlash and possible zero stiffness configuration – justifies considering it as a competitive alternative for conventional mechanical variable stiffness actuators.

Acknowledgements: *This work was funded within the INCARE AAL-2017-059 project „Integrated Solution for Innovative Elderly Care" by the AAL JP and co-funded by the AAL JP countries (National Centre for Research and Development, Poland under Grant AAL2/2/INCARE/2018). The authors would like to thank Mateusz Baczewski and Adam Kowalewski for putting their effort in developing hardware and software used to control drives, register data from encoders and conduct experiments. The authors also wish to express appreciation to Maciej Węgierek for his organisational support and to Katarzyna Kozakiewicz for her help in gathering experimental data and formatting this paper.*

REFERENCES

1. Tsirogiannis, E., Vosniakos, G.-C., 2019, *Redesign and Topology Optimization of an Industrial Robot Link for Additive Manufacturing*, Facta Universitatis Series Mechanical Engineering, 17(3), pp. 415-424.
2. International Federation of Robotics, 2017, *Executive Summary World Robotics 2017 Industrial Robots*, Report World Robotics 2017 Industrial Robots, Frankfurt am Main, Germany, pp. 15-24.
3. Van Damme, M., Beyl, P., Vanderborght, B., Van Ham, R., Vanderniepen, I., Matthys, A., Cherelle, P., Lefeber, D., 2010, *The role of compliance in robot safety*, Proceedings of the Seventh IARP Workshop on Technical Challenges for Dependable Robots in Human Environments, Toulouse, France, pp. 65-71.
4. Walker, D.S., Niemeyer, G., 2010, *Examining the Benefits of Variable Impedance Actuation*, Proc. 2010 IEEE/RSJ International Conference on Intelligent Robots and Systems, Taipei, Taiwan, pp. 4855-4861.
5. Haddadin, S., Laue, T., Frese, U., Wolf, S., Albu-Schäeffer, A., Hirzinger, G., 2009, *Kick it with elasticity: Safety and performance in human robot soccer*, Robotics and Autonomous Systems, 57(8), pp. 761-775.
6. Wolf, S., Hirzinger, G., 2008, *A new variable stiffness design: Matching requirements of the next robot generation*, Proc. 2008 IEEE International Conference on Robotics and Automation, Pasadena, CA, USA, pp. 1741-1746.
7. Bicchi, A., Tonietti, G., 2004, Fast and Soft Arm Tactics: Dealing with the Safety-Performance Trade-Off in Robot Arms Design and Control, IEEE Robotics and Automation Magazine, 11(2), pp. 22-33.
8. Wolf, S., Grioli, G., Eiberger, O., Friedl, W., Grebenstein, M., Höppner, H., Burdet, E., Caldwell, D.G., Carloni, R., Catalano, M.G., Lefeber, D., Stramigioli, S., Tsagarakis, N., Damme, M.V., Ham, R.V., Vanderborght, B., Visser, L.C., Bicchi, A., Albu-Schäffer, A., 2016, *Variable Stiffness Actuators: Review on Design and Components*, IEEE/ASME Transactions on Mechatronics, 21(5), pp. 2418-2430.
9. Braun, D.J., Howard, M., Vijayakumar, S., 2011, *Exploiting Variable Stiffness in Explosive Movement Tasks*, Proc. Robotics: Science and Systems VII, Los Angeles, CA, USA, pp. 25-32.
10. Peacock, J.C.A., Ball, K., 2018, The influence of joint rigidity on impact efficiency and ball velocity in football kicking, Journal of Biomechanics, 71, pp. 245-250.
11. Günther, M., Blickhan, R., 2002, *Joint stiffness of the ankle and the knee in running*, Journal of Biomechanics, 35(11), pp. 1459-1474.
12. Hurst, J.W., Chestnutt, J.E., Rizzi, A.A., 2004, *An actuator with physically variable stiffness for highly dynamic legged locomotion*, Proc. 2004 IEEE International Conference on Robotics and Automation, New Orleans, LA, USA, 5, pp. 4662-4667.
13. Haddadin, S., Weis, M., Wolf, S., Albu-Schäffer, A., 2011, *Optimal Control for Maximizing Link Velocity of Robotic Variable Stiffness Joints*, IFAC Proceedings Volumes, 44(1), pp. 6863-6871.
14. Visser, L.C., Stramigioli, S., Bicchi, A., 2011, *Embodying Desired Behavior in Variable Stiffness Actuators*, IFAC Proceedings Volumes, 44(1), pp. 9733-9738.
15. Visser, L.C., Carloni, R., Stramigioli, S., 2010, *Energy Efficient Control of Robots with Variable Stiffness Actuators*, IFAC Proceedings Volumes, 43(14), pp. 1199-1204.
16. Hurst, J.W., Chestnutt, J.E., Rizzi, A.A., 2010, *The actuator with mechanically adjustable series compliance*, IEEE Transactions on Robotics, 26(4), pp. 597-606.
17. Hogan, N., 1984, *Adaptive control of mechanical impedance by coactivation of antagonist muscles*, IEEE Transactions on Automatic Control, 29(8), pp. 681-690.
18. Vanderborght, B., Albu-Schaeffer, A., Bicchi, A., Burdet, E., Caldwell, D.G., Carloni, R., Catalano, M., Eiberger, O., Friedl, W., Ganesh, G., Garabini, M., Grebenstein, M., Grioli, G., Haddadin, S., Hoppner, H., Jafari, A., Laffranchi, M., Lefeber, D., Petit, F., Stramigioli, S., Tsagarakis, N., Van Damme, M., Van Ham, R., Visser, L.C., Wolf, S., 2013, *Variable impedance actuators: A review*, Robotics and Autonomous Systems, 61(12), pp. 1601-1614.
19. Winiarski, T., Dudek, W., Stefańczyk, M., Zieliński, Ł., Giełdowski, D., Seredyński, D., 2020, *An intent-based approach for creating assistive robots' control systems*, arXiv preprint arXiv:2005.12106.
20. Dudek, W., Winiarski, T., 2020, *Scheduling of a Robot's Tasks With the TaskER Framework*, IEEE Access, 8, pp. 161449-161471.
21. Guiochet, J., Machin, M., Waeselynck, H., 2017, *Safety-critical advanced robots: A survey*, Robotics and Autonomous Systems, 94, pp. 43-52.
22. Haddadin, S., Albu-Schäffer, A., Hirzinger, G., 2009, *Requirements for safe robots: Measurements, analysis and new insights*, The International Journal of Robotics Research, 28(11-12), pp. 1507-1527.
23. Winiarski, T., Węgierek, M., Seredyński, D., Dudek, W., Banachowicz, K., Zieliński, C., 2020, *EARL – Embodied Agent-Based Robot Control Systems Modelling Language*, Electronics, 9(2), 379.
24. Seredyński, D., Winiarski, T., Zieliński, C., 2019, *FABRIC: Framework for Agent-Based Robot Control Systems*, Proc. 12th International Workshop on Robot Motion and Control, Poznań, Poland, pp. 215-222.

25. De Schutter, J., Bruyninckx, H., Zhu, W.-H., Spong, M.W., 1998, *Force control: a bird's eye view*, Proc. Control Problems in Robotics and Automation, San Diego, CA, USA, pp. 1-17.
26. Kornuta, T., Zieliński, C., Winiarski, T., 2020, *A universal architectural pattern and specification method for robot control system design*, Bulletin of the Polish Academy of Sciences: Technical Sciences, 68(1), pp. 3-29.
27. Winiarski, T., Woźniak, A., 2013, *Indirect force control development procedure*, Robotica, 31(3), pp. 465-478.
28. Zieliński, C., Winiarski, T., 2010, *Motion Generation in the MRROC++ Robot Programming Framework*, The International Journal of Robotics Research, 29(4), pp. 386-413.
29. Winiarski, T., Walęcki, M., 2014, *Motor cascade position controllers for service oriented manipulators*, Proc. Recent Advances in Automation, Robotics and Measuring Techniques, Warsaw, Poland, pp. 533-542.
30. Albu-Schaeffer, A., Haddadin, S., Ott, C., Stemmer, A., Wimböck, T., Hirzinger, G., 2007, *The DLR lightweight robot: Design and control concepts for robots in human environments*, Industrial Robot, 34(5), pp. 376-385.
31. Knox, B.T., Schmiedeler, J.P., 2009, *A Unidirectional Series-Elastic Actuator Design Using a Spiral Torsion Spring*, Journal of Mechanical Design, 131(12), 125001.
32. Sugar, T.G., 2002, *A novel selective compliant actuator*, Mechatronics, 12(9-10), pp. 1157-1171.
33. Van Ham, R., Sugar, T.G., Vanderborght, B., Hollander, K.W., Lefeber, D., 2009, *Compliant actuator designs*, IEEE Robotics Automation Magazine, 16(3), pp. 81-94.
34. Tagliamonte, N.L., Sergi, F., Accoto, D., Carpino, G., Guglielmelli, E., 2012, *Double actuation architectures for rendering variable impedance in compliant robots: A review*, Mechatronics, 22(8), pp. 1187-1203.
35. Qian, K.-X., Zeng, P., Ru, W.-M., Yuan, H.-Y., 2003, *Novel magnetic spring and magnetic bearing*, IEEE Transactions on Magnetics, 39(1), pp. 559-561.
36. Garbin, N., Di Natali, C., Buzzi, J., De Momi, E., Valdastri, P., 2015, *Laparoscopic Tissue Retractor Based on Local Magnetic Actuation*, Journal of Medical Devices, 9(1), 011005.
37. Sun, F., Zhang, M., Jin, J., Duan, Z., Jin, J., Zhang, X., 2016, *Mechanical analysis of a three-degree of freedom same-stiffness permanent magnetic spring*, International Journal of Applied Electromagnetics and Mechanics, 52, pp. 667-675.
38. Robertson, W., Cazzolato, B., Zander, A., 2005, *A multiple array magnetic spring*, IEEE Transactions on Magnetics, 41(10), pp. 3826-3828.
39. Zhang, M., Fang, L., Sun, F., Sun, X., Gao, Y., Oka, K., 2018, *Realization of Flexible Motion of Robot Joint with A Novel Permanent Magnetic Spring*, Proc. 2018 IEEE International Conference on Intelligence and Safety for Robotics, Shenyang, China, pp. 331-336.
40. Xu, X., Zeng, C., 2013, *Magnetic Spring and Experimental Research on its Stiffness Properties*, Advanced Materials Research, 706-708, pp. 1418-1422.
41. Sudano, A., Tagliamonte, N.L., Accoto, D., Guglielmelli, E., 2014, *A resonant parallel elastic actuator for biorobotic applications*, Proc. 2014 IEEE/RSJ International Conference on Intelligent Robots and Systems, Chicago, IL, USA, pp. 2815-2820.
42. Choi J., Park, S., Lee W., Kang S.-Ch., 2008, *Design of a robot joint with variable stiffness*, Proc. 2008 IEEE International Conference on Robotics and Automation, Pasadena, CA, USA, pp. 1760-1765.
43. Yoo, J., Hyun, M.W., Choi, J.H., Kang, S., Kim, S.-J., 2009, *Optimal design of a variable stiffness joint in a robot manipulator using the response surface method*, Journal of Mechanical Science and Technology, 23(8), pp. 2236-2243.
44. Sudano, A., Accoto, D., Zollo, L., Guglielmelli, E., 2013, *Design, Development and Scaling Analysis of a Variable Stiffness Magnetic Torsion Spring*, International Journal of Advanced Robotic Systems, 10(10), 372.
45. Spong, M.W., 1987, *Modeling and Control of Elastic Joint Robots*, Journal of Dynamic Systems, Measurement, and Control, 109(4), pp. 310-318.
46. Flacco, F., 2012, *Modeling and control of robots with compliant actuation*, PhD Thesis, SAPIENZA Università di Roma, Italy.
47. Albu-Schäffer, A., Ott, C., Hirzinger, G., 2007, *A Unified Passivity-based Control Framework for Position, Torque and Impedance Control of Flexible Joint Robots*, The International Journal of Robotics Research, 26(1), pp. 23-39.
48. Benhama, A., Williamson, A.C., Reece, A.B.J., 2000, *Virtual work approach to the computation of magnetic force distribution from finite element field solutions*, IEE Proceedings – Electric Power Applications, 147(6), pp. 437-442.